Bioelectrochemistry 112 (2016) 112–124

Contents lists available at ScienceDirect

Bioelectrochemistry

journal homepage: www.elsevier.com/locate/bioelechem

Properties of lipid electropores II: Comparison of continuum-level modeling of pore conductance to molecular dynamics simulations

Lea Rems [a,1], Mounir Tarek [b,c,*], Maura Casciola [b,d,e], Damijan Miklavčič [a]

[a] Faculty of Electrical Engineering, University of Ljubljana, Tržaška 25, SI-1000 Ljubljana, Slovenia
[b] SRSMC, UMR 7565, Université de Lorraine, Vandoeuvre-lès-Nancy, F-54506, France
[c] SRSMC, UMR 7565, CNRS, Vandoeuvre-lès-Nancy, F-54506, France
[d] Department of Information Engineering, Electronics and Telecommunications (D.I.E.T.), Sapienza University of Rome, 00184 Rome, Italy
[e] Center for Life Nano Science@Sapienza, Istituto Italiano di Tecnologia, 00161, Rome, Italy

ARTICLE INFO

Article history:
Received 30 October 2015
Received in revised form 24 March 2016
Accepted 27 March 2016
Available online 6 April 2016

Keywords:
Electroporation
Lipid bilayer
Pore conductance
Molecular dynamics simulations
Poisson–Nernst–Planck theory

ABSTRACT

Electrical conductance of an aqueous pore in the lipid bilayer has an important role in the process of membrane electroporation, i.e., formation of pores induced by electric pulses. In our present study we compare the pore conductance as predicted by a theoretical model based on the continuum Poisson–Nernst–Planck theory to the pore conductance obtained with molecular dynamics simulations (Casciola et al., Bioelectrochemistry 109:108–116, 2016). Our analysis demonstrates that the Poisson–Nernst–Planck model is able to quantitatively predict the dependence of the pore conductance on the pore radius when considering the toroidal shape of the pore. In order to correctly describe the difference in the pore conductance for Cl and Na ions (the pore selectivity), however, it is necessary to take into account the electric double layer next to the lipid–water interface and the electroosmotic flow through the pore. We further show that simplified analytical descriptions of pore conductance can lead to incorrect predictions of the pore size extracted from experimental measurements, and can affect the predictions of electroporation models. Overall, this study demonstrates that continuum modeling can be efficiently used as complementary method to molecular scale models for investigating lipid pores.

1. Introduction

Electroporation, known as a method of breaching the cell membrane barrier by means of electric pulses, has been found valuable in numbers of applications in very different scientific and technological fields: medicine [1–5], food processing and food preservation [6–10], biofuel production [9,11], as well as water decontamination [12,13]. Despite its widespread use, our understanding of electroporation at the molecular level of the membrane itself still lacks a complete picture [14–17]. Consequently, the state of the art of current theoretical models of electroporation may not be at sufficiently high level and further research is necessary in order to develop models that will be able to correctly interpret or predict experimental outcomes.

Theoretical models which are used to describe electroporation on the scale of single cells or cell clusters are based on continuum approaches and are therefore often referred to as continuum electroporation models [18,19]. In continuum description, the molecular structure is neglected and the membrane is simply viewed as a thin homogenous dielectric layer surrounded by an electrolyte solution. Such models constitute an important part of electroporation research as they enable exploration on length scales (more than hundreds of micrometers) and time scales (seconds and more) currently not achievable by molecular dynamics (MD) simulations or molecular models based on the mean field theory [20–22]. Note that the diameters of mammalian cells are of the order of 10 μm and the time scales, over which structural changes in the membrane due to electroporation can be observed, range from nanoseconds to minutes or even hours [14]. Continuum models have indeed considerably contributed to our understanding of electroporation under different experimental conditions [23–28]. They can be probed to give the information on the time course and magnitude of the induced transmembrane voltage, as well as the electric field distribution inside and outside of a model cell or cell cluster [29]. To certain extent, they can even be used to predict the number and size of pores in the membrane and the rate of molecular transmembrane transport [30–33]. Hence, they provide a valuable tool for explaining certain experimental observations or for tailoring the experimental protocol in order to give an optimal result [34].

The general physical concept embedded in continuum electroporation models is rather simple: the transmembrane voltage, which is induced across the membrane by an electric pulse, reduces the energetic barrier for nucleation of small aqueous pores in the lipid bilayer [18]. The induced transmembrane voltage (more specifically the

* Corresponding author at: CNRS, Unité Mixte de Recherches 7565, Université de Lorraine, Boulevard des Aiguillettes, BP 70239, 54506 Vandoeuvre-lès-Nancy, France.
E-mail address: mounir.tarek@univ-lorraine.fr (M. Tarek).
[1] Present address: Department of Chemical Engineering, Delft University of Technology, 2628BL Delft, The Netherlands.

http://dx.doi.org/10.1016/j.bioelechem.2016.03.005
1567-5394/

corresponding induced electric field in the membrane) also provides a force which tends to expand the formed pores [35]. As the expanding pores start to conduct more and more ions, the voltage across the membrane effectively reduces, which in turn limits further pore creation and expansion [25,36]. Theoretical description of pore conductance therefore plays an important role in electroporation models as it implicitly controls the dynamics of the transmembrane voltage and thereby the number and size of membrane pores.

Apart from its importance in electroporation models, theoretical description of pore conductance also provides a convenient way to characterize pore properties from experimental measurements. Pore conductance namely depends on the pore size, geometry, as well as the surface properties of the pore wall, such as the surface charge. By analyzing the measurements with a theoretical model, it is possible to gain information on the pore size [37–40] or other structural characteristics, such as geometrical asymmetry, which (together with surface charge on the pore wall) manifests itself in ionic current rectification [41]. Geometrical asymmetry of lipid pores could for example arise from asymmetric lipid composition, which is present in cell membranes [42,43].

Measurements of pore conductance are particularly convenient for characterization of pore properties since there are at present no experimental techniques allowing direct visualization of small lipid pores in nanometer or subnanometer resolution, required to accurately capture the pore size and geometry. Lipid pores are namely highly dynamic, with their size and stability being strongly dependent on the transmembrane voltage [44–47]. There have been several attempts to measure the pore size by monitoring the transmembrane transport of molecules with different size (e.g. propidium iodide, YO-PRO-1, bleomycin, trypan blue, PEG, sugar molecules, and dextrans; for a short review see [48]), particularly in electroporation experiments on cells. However, the reliability of this method remains uncertain, since charged and sugar molecules can strongly interact with the lipid bilayer and could therefore perturb the pore configuration while translocating through the pore [49,50]. For this reason, conductance measurements provide more sensitive and less perturbing method to characterize the properties of lipid pores. Moreover, the transport of molecules across cell membranes generally needs to be monitored during seconds or minutes after applying electric pulses, whereby the exact molecular mechanisms of the increased cell membrane permeability in this post-pulse membrane resealing phase have not yet been clearly elucidated [17,51].

For accurate characterization of the pore properties from conductance measurements it is necessary to have a valid and reliable theoretical model, which can quantitatively predict the pore conductance. Furthermore, reliable model of pore conductance is necessary in continuum electroporation models, in order to adequately predict the number and size of pores, as discussed above.

Typically, ionic conduction through lipid pores is theoretically described by means of more or less simplified expressions, which in its core derive from the coupled Nernst–Planck and Poisson's equations [52–54]. The Nernst–Planck equations describe the electro-diffusion of ions in terms of ionic concentration, where the driving force for the electrophoretic drift – the gradient in the electric potential – is given by the Poisson's equation. The so-called Poisson–Nernst–Planck (PNP) theory is a general and well-established continuum approach to analyze ionic transport in many different fields including research on ion channels and nanochannels [55–59], both closely related to lipid pores investigated in this study.

For descriptions of ionic transport through ion channels the PNP theory has some known limitations, which mainly arise from treating the ions as point charges and neglecting the ion–ion correlations. These limitations are particularly expressed in narrow channels with radii of less than 2–3 Debye lengths [60,61], where the mean field approximation breaks down. For example, the PNP theory allows a certain concentration of ions to be found in a channel, albeit the channel is too narrow to actually fit a finite-size ion. A direct consequence is an overestimate of the electrolytic shielding effects and an underestimate of the repulsive image forces induced in the dielectric channels walls [62], for which the PNP theory usually systematically predicts higher ionic current than the corresponding molecular scale models [61–63].

Indeed, continuum theories are designed to be used in systems containing a large number of ions, so it is not unexpected that the PNP theory will fail to accurately predict ionic current in channels, where only a single or a few ions can be found at a certain moment [61,62]. In such cases, methods that treat the ions explicitly give more reliable results. Atomistic MD simulations provide the most general platform, because they take into account the entire atomistic structure of the investigated system (e.g. the ion channel and its immediate surroundings), but are for the same reason also computationally extremely demanding. Alternative methods such as Brownian dynamics simulations have thus been proposed, where the channel and ions are represented explicitly at the atomic level, whereas the surrounding solvent is treated as featureless dielectric medium incorporated implicitly via stochastic random forces and multi-ion potential of mean force [56,63]. Such methods were shown to provide better agreement with experiment as compared to the PNP theory [55,62,63].

Nevertheless, continuum theories still offer considerably simpler and less time consuming method to study ionic transport [57]. Therefore, great efforts have been made to modify the PNP equations in order to better capture the physics of particles in confined channels [62]. The problem of the finite size of ions has been addressed by including ion repulsion using the hard sphere chemical potential from the density functional theory of inhomogeneous liquids [64–67], or the Lennard-Jones repulsive potential [67–69]. Alternatively, the PNP theory was upgraded by implicitly including the solvent and empty spaces (void volume) between particles as separate species in the electrolyte in addition to ions [70]. The down side of increasingly complex modifications is, though, that they considerably hamper numerical implementations and require specific numerical algorithms to solve the equations [71].

The first objective of our study is to verify whether the PNP theory in its original form can satisfactorily describe the conductance of a pore in the lipid bilayer. MD simulations performed in our preceding paper [46] provide an excellent opportunity to achieve this objective for two main reasons. Firstly, MD simulations enable one to directly and independently characterize the pore conductance, pore size, and pore geometry [45], which is impossible to achieve with current experimental techniques. Secondly, the simulations were performed using a specific algorithm, which allows one to observe stable pores in the bilayer and enables thorough characterization of their properties. As explained in greater detail by Casciola et al. [46], the simulations were specifically tailored to mimic typical experimental conditions in electroporation as much as possible. A different, though related approach to characterize the conductance of stable lipid pores using MD simulations was already done by Ho et al. [45], however, their results have not been systematically analyzed from the perspective of the continuum PNP theory.

The second objective of our study is to check to what extent do simplified theoretical expression of pore conductance affect the estimates of the pore size from experimental measurements and predictions arising from continuum electroporation models. Both in experimental and theoretical studies of electroporation, the descriptions of pore conductance are generally based on simplified assumptions of cylindrical pore geometry as well as a one-dimensional approximation of the flux of ions across the pore [52–54].

The paper is organized as follows. In Methods we first focus on certain observations from MD simulations, which directed the development of our PNP model of ionic conduction through a lipid pore from its basic form to further upgrades. Afterwards we describe the PNP model in detail. In Results and discussion we compare the pore conductance as well as the electric potential and ionic concentration profiles as obtained from MD simulations and as predicted by the model that we developed. We then continue with discussion on the applicability of

the existing analytical derivations of pore conductance used for the determination of pore size from experimental measurements as well as for their use in continuum electroporation models, and end with a concluding remark in Conclusions.

2. Methods

We constructed the PNP model of ionic current flowing through a lipid pore based on the finite element method (FEM) in COMSOL Multiphysics 5.0. Our "basic PNP model", which we use as a starting point, closely relates to the one proposed by Li and Lin [54], who analytically derived the expression for the conductance of a cylindrical pore in the general case of unequal ionic concentration on each side of the membrane using the PNP theory. However, we avoid certain simplifications which were required in [54] in order to obtain an analytical derivation, and adapt the model to correspond more closely to the MD system studied. Three major differences can be found: (i) Li and Lin considered that the source of the electric potential is infinitely far away from the pore, hence modeling an infinitely large system, whereas we adapt the model domain to the size of the MD system; (ii) we approximate the pore shape as toroidal instead of cylindrical, which is a more reasonable approximation for pores observed in the MD simulations (Fig. 1a); (iii) we consider that the anions and cations (in our case Na and Cl ions) have different diffusion coefficients, which moreover depend on the ionic concentration, as found experimentally [72]; whereas Li and Lin assumed that the diffusion coefficient is equal for both species and constant regardless of the ionic concentration.

It is important to stress that our model is closely adapted to the MD system; we extracted all relevant model parameters directly from the MD trajectories or by performing additional independent simulations. By that we could ensure that any disagreement between the results obtained in the simulations and with the PNP model could straightforwardly be attributed either to the limits of the validity of the PNP theory or to some missing elements in the model. Indeed we found that our basic PNP model itself cannot fully capture all of the underlying physics in ionic conduction through the pore. The findings of our study are though not limited to the MD system, but are applicable to any similar experimental system.

To avoid confusion, we consistently use the term "MD system" to refer to the atomistic system with which MD simulations were performed, and the term "FEM model" to refer to the PNP model developed based on the results from MD simulations. For brevity we avoid any technical details of the model implementation into the COMSOL environment, as well as the data extraction from MD simulations. For such information we kindly refer the reader to the Supplementary Material.

2.1. Brief description of MD simulations

The system in MD simulations, which are described in detail in our preceding paper [46], consisted of a lipid bilayer made from 1-palmitoyl-2-oleoyl-*sn*-glycero-3-phosphocholine (POPC) molecules, bathed in ~1 M NaCl solution and maintained at temperature of 300 K. The bilayer also contained a preformed pore in its center (Fig. 1a). In order to calculate the electric current through the pore, the simulations were run in GROMACS suite using a specific swapping algorithm that maintains a constant charge imbalance across the pore. The algorithm is namely designed such that when an ion crosses the pore from the region A above the bilayer to the region B below the bilayer, a different ion (of the same type) from region B is swapped with a water molecule from region A (or vice versa). Since periodic boundary conditions are applied on all sides of the simulation box, a vacuum layer is present between the region A and B, which ensures that the ions can move between regions solely through the pore. The number of positive and negative ions above and below the bilayer is thus maintained and is not influenced by the ionic current flowing through the pore. If we initially put an excess number of Na ions above the bilayer and a corresponding excess number of Cl ions below the bilayer, the algorithm will maintain this charge imbalance throughout the simulation resulting in relatively steady transmembrane voltage sustaining the pore. In addition, the surface tension of the bilayer is maintained at ~0 mN/m, allowing the pore to freely adapt its size. The size of the pore, however, influences the ionic current through the pore as well as the electric potential gradient across the simulated system. Hence, the pore radius, the electric current, and the transmembrane voltage are all "free" parameters, which can spontaneously adapt as the system moves towards an energetic minimum.

For the theoretical analysis reported here, we use the results obtained with the system made from 1024 POPC molecules. These simulations were performed for five constant charge imbalances, i.e., $20q_e$, $32q_e$, $40q_e$, $48q_e$, and $56q_e$ (q_e is the elementary charge), as well as for a system without charge imbalance and without a pore ($0q_e$). The analysis of the MD results in this study though deviates from the one used in [46]. We namely took into account that the typical time scale of charge relaxation in an electrolyte with conductivity $\sigma_e \approx 9$ S/m, which corresponds to ~1 M NaCl in our MD system, is estimated to be $\tau_r = \varepsilon_e\varepsilon_0/\sigma_e \approx 80$ ps [54], where $\varepsilon_e \approx 80$ is the relative dielectric permittivity of the

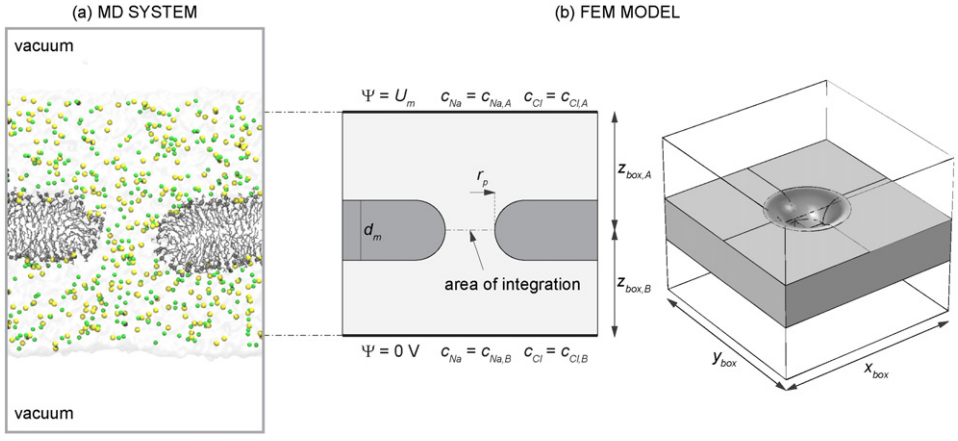

Fig. 1. MD system and corresponding FEM model. (a) Slice across the central region of the MD system. Na ions and Cl ions are presented in yellow and green, respectively, the lipids are in gray with phosphate atoms shown as spheres. Water is shown as light gray surface. The gray rectangle indicates the dimensions of the simulation box in *x* and *z* direction. (b) Slice across the center of the FEM model (left) and 3D view of the model (right). Lipid bilayer is shown in dark gray. The boundaries of the FEM model at the top and bottom side correspond to the *z* planes in the MD system, where bulk properties of the electrolyte are established. The dimensions of the FEM model in *x* and *y* are equal to the dimensions of the MD system.

electrolyte and ε_0 the permittivity of vacuum. Therefore, we can safely assume that, in terms of electrostatics, a stationary electric current is established very fast with respect to the time scale of the simulations, and any changes in the pore conductance are simply caused by slower changes in the pore size. Since the pore size is slightly changing throughout all simulations, we divided each 80 ns long trajectory into four 20 ns long parts and analyzed them separately with respect to the transmembrane voltage, the ionic current, and the pore radius. By averaging the analyzed variables over every 20 ns long part, we could obtain 20 data points describing how the pore conductance depends on the pore radius. This enables a more detailed analysis as compared to the one based on averages over 60 ns extracted from each of the simulations performed at different charge imbalances [46]. Indeed we observed that regardless of the charge imbalance imposed, the dependence of the calculated pore conductance on the pore radius falls on the same curve (see e.g. Fig. 3), corroborating our approach of data analysis.

2.2. Note on the net water flow

An important factor that could influence the overall ionic current through the pore is a net water flow we observed in all simulations. The water flow is quite steady, is directed opposite to the electric field, i.e. in the direction of the flow of Cl ions, and increases with increasing charge imbalance imposed in simulations (Fig. 2a).

The water flow can be attributed to electroosmosis, a phenomenon technologically widely exploited in micro- and nano-fluidics to drive fluids through channels by means of an electric field instead of a pressure gradient [73,74], or to modulate flow of macromolecules such as DNA through solid-state nanopores [75]. These channels and nanopores are designed to have a charged inner surface and hence an interfacial electric double layer which results in charge separation at the interface. The electric field applied parallel to the double layer can thus produce a net force on the mobile counterions. The induced motion of counterions produces a viscous drag force on the surrounding bulk liquid that exceeds the opposing force of the less plentiful coions [76]. The resulting net force on the fluid then induces a bulk fluid motion known as electroosmosis.

Although POPC lipids are zwitterionic and do not have a net surface charge, the Na ions have a higher affinity to bind to negatively charged oxygen atoms of the lipid headgroups compared to the affinity of Cl ions to bind to positively charged nitrogen atoms, thereby acting similarly as surface charge (we must note here that the higher binding affinity of Na ions is specifically observed in MD simulations, though a recent study suggests that it may be an artifact of the force fields and that the binding affinities of Na and Cl to lipids are more similar [77]). An electric double layer is therefore formed at the lipid–water interface, which is also present inside the pore. This can be seen in Fig. 2c, which shows a 2D profile of the difference in concentration of Cl and Na ions. The coordinate system is placed in the center of the pore, where coordinate r corresponds to the horizontal and coordinate z to the vertical distance from the center (we use an axisymmetric coordinate system; see figure caption and Supplementary Material Section S2.8 for more details). Note that there is a layer of excess Na ions surrounded by a layer of excess Cl ions along the entire lipid–water interfacial region. Though Na ions are not bound permanently and can contribute to the Na current through the pore, there is a steady number of bound Na ions in the pore wall which influences the electrostatics inside the pore and, as will be shown by results, enhances the conductance of the pore to Cl ions.

On the molecular scale, there are two mechanisms of net water transport in the presence of an electric field, which are captured in MD simulations [78]. The first is the transfer of the momentum from electrophoretically driven ions to neutral water molecules during collisions. The second mechanism is the drag of water molecules, which are associated to moving ions. The Cl ions have higher mass and higher diffusion coefficient, and therefore a higher momentum than Na ions, as well as a higher coordination number and are thereby associated with a higher number of water molecules. In our MD system, the bulk diffusion coefficients of Cl and Na ions in 1 M NaCl are $1.5 \cdot 10^{-9}$ m^2/s and $1.0 \cdot 10^{-9}$ m^2/s, respectively (see Supplementary Material Section S2.5). The coordination numbers of Cl and Na ions are 7.8 and 5.3, respectively, as obtained from the radial distribution functions. The residence time of water in the first hydration shell in the absence of electric field, which we calculated following [79], is though shorter for Cl; namely 14 ps for Cl and 40 ps for Na. Hence the "transfer of momentum" mechanism should be dominated by Cl ions, whereas the "dragging" mechanism should actually be dominated by Na ions due to much longer water residence time. Nevertheless, as considerably larger number of Cl ions pass the pore, their number dominance apparently unequivocally determines the direction of the water flow.

The net water flow has two consequences that may influence the electric current through the pore. The first is the change in the overall ionic concentration profile below and above the bilayer, which is a direct consequence of the finite size of the MD system. As the system is canonical, the net water flow results in gradual decrease of the water volume below the bilayer and concomitant increase in the water volume above the bilayer. The swapping algorithm though maintains the number of ions (but not water) below and above the bilayer constant. The changes in water volume hence result in increase/decrease in the bulk NaCl concentration below/above the bilayer (Fig. 2b). The induced concentration gradient could result in diffusive current through the pore. The typical time scale for diffusion can be

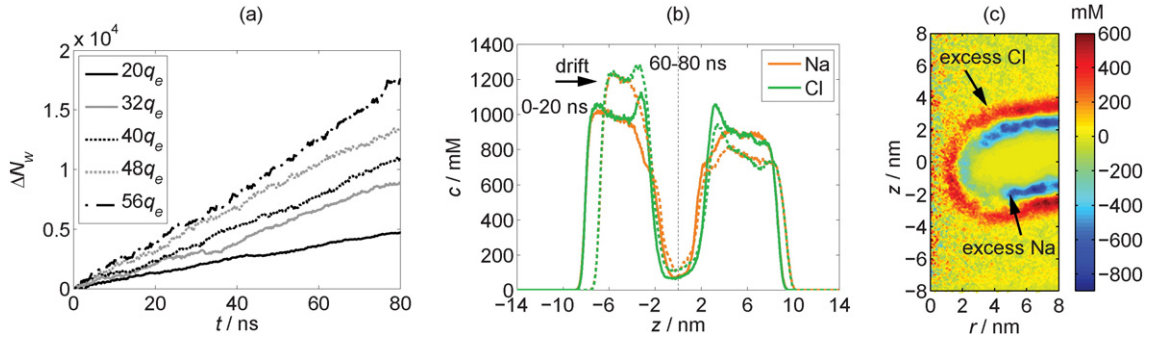

Fig. 2. Net water flow. (a) Increase in the number of water molecules ΔN_w above the center of the bilayer with time, with respect to the beginning of the simulation. (b) Changes in the concentration profiles along the vertical axis of the MD system due to net water flow. The profiles are shown for charge imbalance $48q_e$, and were obtained as an average over the first 20 ns (solid lines) and the last 20 ns (dotted lines) of the trajectory. The center of the bilayer is indicated with vertical dotted line. The concentration of ions below the bilayer increases, whereas the concentration above the bilayer decreases with time. (c) Difference in concentration of Cl and Na ions at the lipid–water interface. The profile was obtained by extracting the positions of ions from one of the trajectories and transforming Cartesian coordinates (x, y, z) into axisymmetric cylindrical coordinates (r, z) by placing the center of the cylindrical coordinate system at the center of the pore.

expressed as $\tau_D = L^2/D$, where L is a typical distance and D is the diffusion coefficient [54]. For Cl ions with diffusion coefficient $D_{Cl} = 1.5 \cdot 10^{-9}$ m/s^2 passing through a ~4 nm thick membrane $\tau_D =$ ~11 ns, which is within the timescale of the MD simulations (80 ns), as well as within the 20 ns long piece of trajectory that was analyzed separately. In addition, the concentration gradient across the bilayer could influence the distribution of ions and consequently the electrostatics around the pore [54].

The second consequence of the water flow is a convective ionic current induced by the net fluid motion. The fluid flows in the direction of Cl ions and contributes to the electrophoretic Cl current, whereas it opposes the Na electrophoretic current. The order of magnitude of this contribution can be estimated from the mass flow rate of water through the pore:

$$\frac{\Delta m_w}{\Delta t} = \frac{\Delta N_w}{\Delta t}\frac{M_w}{N_A} = \rho_w \frac{\Delta V_w}{\Delta t} \tag{1}$$

where $\Delta N_w/\Delta t$ is the number of water molecules passing through the pore per unit time (slope of curves in Fig. 2a), $M_w = 18$ g/mol is the molar mass of a water molecule, and N_A is the Avogadro constant. The mass flow rate can then be related to the volumetric flow rate by scaling it with the water density $\rho_w = 972$ kg/m^3 (calculated from the density profile of water in the MD system). Since the overall volume of water is much larger than the volume of solvated ions (in the MD system the fraction of ions in the electrolyte is ~3%), we can consider that the volume of fluid (water and ions) is simply equal to the volume of water, hence $\Delta V_w = \Delta V$. The volumetric fluid flow rate $\Delta V/\Delta t$ can now be related to the convective electric current. The electric current I_i of ions of type i through the pore is defined as the number of charges $q_e z_i \Delta N_i$ passing through the pore per unit time. If we express the number of ions in terms of ionic concentration $\Delta N_i = c_i N_A \Delta V$, we find that

$$I_i = q_e z_i c_i N_A \frac{\Delta V}{\Delta t} \approx \frac{q_e z_i c_i M_w}{\rho_w}\frac{\Delta N_w}{\Delta t}. \tag{2}$$

A simple calculation for a flow rate of 150 water molecules per ns and 1 M ionic concentration gives a convective electric current of ± 0.5 nA. Though this is rather small compared to the total measured electric current (up to ~4 nA for Na and ~12 nA for Cl), the convective current may notably contribute to the higher pore conductance for Cl ions than for Na ions, which was seen in MD simulations (note that we term the higher pore conductance for Cl than Na ions "the pore selectivity" as is custom in ion channels [66,55,73]).

According to these observations we decided to perform calculations for three increasingly complex variants of the FEM model. In FEM model 1 (our "basic PNP model") we neglect the electric double layer and the electroosmotic fluid flow, which is custom when describing pore conductance in continuum electroporation models. In FEM model 2 we include the electric double layer by modeling the bound Na ions as surface charge at the lipid–water interface. In FEM model 3 we add also the fluid flow by coupling the Poisson–Nernst–Planck equations with Navier–Stokes equation. Comparison between the three models allows us to separately evaluate the contribution of the electric double layer and the fluid flow on the pore conductance and particularly on pore selectivity for Cl ions.

In addition we use two different sets of model parameters. In the first set we consider a simplified system, where we only vary the pore radius, and we keep the size of the system completely symmetric, with equal volume and ionic concentration below and above the bilayer, corresponding to the initial point of the simulations, and use equal transmembrane voltage for all pore radii. In this parameter set we also neglect the dependence of the diffusion coefficient of ions on ionic concentration. In the second set we adapt the size of the electrolyte volume and the ionic concentration below and above the bilayer, the transmembrane voltage, and the pore radius exactly as was extracted from each 20 ns part of the MD trajectories, and moreover take into account that the diffusion coefficients of ions depend on the ionic concentration (further details can be found in the Supplementary Material). We name a model with the first set of parameters as "symmetric", and a model with the second set as "asymmetric". Comparison of calculations from these two sets of parameters allows us to evaluate the influence of geometry and concentration gradient across the bilayer on the overall results, as well as the required complexity of the model to capture the essential features of ion conduction through the pore.

2.3. Finite element model

2.3.1. Geometry

The lipid bilayer is represented by a slab with thickness d_m, which contains a pore in its center (Fig. 1b). The membrane thickness was extracted from the distance between the peaks in density distribution of phosphorus atoms in the MD system with $0q_e$ charge imbalance. The shape of the pore was always modeled as toroidal except in one set of calculations, where we investigated the effect of the pore shape on the calculated pore conductance. The radius of the narrowest part of the pore is defined as the pore radius r_p (this directly corresponds to the way how the pore radius was extracted from MD simulations, see Supplementary Material Section S2.1). The bilayer is embedded in a cuboidal box with dimensions x_{box}, y_{box}, z_{box}, which represents the electrolyte. An important consideration that we make is that we neglect the vacuum layer present in the MD system, which is required to maintain a constant charge imbalance across the bilayer. Instead, we "cut" the MD system at horizontal planes below and above the bilayer where the "bulk" properties of the electrolyte are established. At these planes we use Dirichlet boundary conditions, which are extracted from the MD system (see below).

2.3.2. Physics

As already noted, we performed calculations for three increasingly complex variants of the FEM model. The description given here is for the most complex variant (FEM model 3) where we take into account the electric double layer at the lipid–water interface and the electroosmotic fluid flow through the pore. This model is based on coupled Nernst–Planck, Poisson, and Navier–Stokes equations. The lipid bilayer is only passively included in the model through boundary conditions at the lipid–water interface. Although we performed separate calculations including the bilayer as a nonconductive dielectric with relative permittivity $\varepsilon_l = 2$, we found that this has negligible effect on the results, as has already been observed previously [54].

In the electrolyte, the concentration of Na and Cl ions are described by the steady-state Nernst–Planck equations

$$\mathbf{j_i} = -D_i \nabla c_i - D_i \frac{z_i q_e}{kT} c_i \nabla \Psi + \mathbf{v} c_i \tag{3a}$$

$$\nabla \mathbf{j_i} = 0 \tag{3b}$$

where subscript i corresponds to either Na or Cl. Variables $\mathbf{j_i}$, c_i, Ψ, and $\mathbf{v}$ are the molar flux of ions, concentration in mol/m^3, electric potential, and fluid velocity, respectively. Constants $z_i = \pm 1$, q_e, k, and $T = 300$ K are the valence of ions, elementary charge, Boltzmann constant, and absolute temperature, respectively. The values of diffusion coefficients D_i and their dependence on ionic concentration were extracted from MD simulations (see Supplementary Material Section S2.5). The first term describing the molar flux $\mathbf{j_i}$ accounts for ionic diffusion, the second for electrophoresis, and the third for convection.

The electric potential distribution is given by the Poisson's equation

$$\varepsilon_e \varepsilon_0 \Delta \Psi = -\rho_e \tag{4a}$$

$$\rho_e = F(z_{Na} c_{Na} + z_{Cl} c_{Cl}) \tag{4b}$$

where ρ_e is the charge density, $\varepsilon_e = 80$ and ε_0 relative permittivity of the electrolyte and permittivity of vacuum, respectively, and F is the Faraday constant. Note that the relative dielectric permittivity of the TIP3P water model, which was used in the MD system, is about ~86 at 300 K [80], but in the presence of ions the permittivity decreases, experimentally to about 70 in 1 M NaCl [81]. Therefore we tested whether the value of the permittivity has a profound effect on the results. In addition to using $\varepsilon_e = 80$ we performed calculations also for $\varepsilon_e = 70$ and 60; however, the difference in results was not significant (up to 2% difference in the calculated total pore conductance for $\varepsilon_e = 70$ and up to 5% for $\varepsilon_e = 60$).

The fluid velocity is given by Navier–Stokes equation for incompressible flow

$$\rho_w(\mathbf{v}\cdot\nabla)\mathbf{v} = \nabla\left[-p\mathbf{I} + \eta_w\left(\nabla\mathbf{v} + (\nabla\mathbf{v})^{\mathrm{T}}\right)\right] \tag{5a}$$

$$\nabla\cdot\mathbf{v} = 0 \tag{5b}$$

where p is the pressure and $\mathbf{I}$ identity matrix. The fluid density and dynamic viscosity are taken as the density of water in the MD system $\rho_w = 972$ kg/m^3, and the viscosity of TIP3P water model $\eta_w = 0.321$ mPa·s [82].

Generally, electroosmotic flow is described by adding a source term $-\rho_e\nabla\Psi$ to the right hand side of (5a) [83]. However, we observed that such description considerably overestimates the velocity of fluid and mass flow rate compared to the one seen in the MD system, which has been noted before in the case of nanochannels [76]. The overestimate is inherent to the theory and is mainly caused by neglect of the finite size of ions [76]. To be more close to the MD system with the model, we instead impose a boundary condition defining a constant mass flow rate $\Delta m_w/\Delta t$ from the bottom side of the FEM model

$$-\int_{\partial\Omega}\rho_w(\mathbf{v}\cdot\mathbf{n})\mathrm{dA} = \frac{\Delta m_w}{\Delta t} \tag{6}$$

and a zero stress condition at the opposite side

$$\left[-p\mathbf{I} + \eta_w\left(\nabla\mathbf{v} + (\nabla\mathbf{v})^{\mathrm{T}}\right)\right]\mathbf{n} = 0. \tag{7}$$

The imposed mass flow rate was extracted from the MD system as described in Supplementary Material Section S2.4. Although this approach results in a pressure gradient across the system which is not present in electroosmosis, the velocity profile of the fluid is quite similar, and more importantly, is closer by magnitude to the one in the MD system. As we are primarily testing the applicability of the PNP model to describe lipid pore conductance, we consider out of the scope of the present study to adapt the model of electroosmosis to accurately capture the fluid flow in the MD system, and consider a constant mass flow rate as a reasonable enough approximation. And indeed this is corroborated by results, as presented later.

For concentration and electric potential we use Dirichlet boundary conditions at the top and bottom of the electrolyte, the values of which are extracted from MD simulations (see Supplementary Material Section S2.2). The electric potential at the bottom is arbitrarily set to 0 V; consequently, the electric potential at the top has the value of the transmembrane voltage U_m (Fig. 1b).

At vertical sides of the electrolyte we use "zero flux" boundary conditions for ionic concentration and electric potential, and a "symmetry" condition for velocity

$$\mathbf{n}\cdot\mathbf{j_i} = 0;\quad \mathbf{n}\cdot\nabla\Psi = 0;\quad \mathbf{v}\cdot\mathbf{n} = 0. \tag{8}$$

Since the model geometry is left–right symmetrical, the zero flux and symmetry boundary conditions mimic the situation where the model would be replicated in the horizontal directions, which is similar to the implementation of periodic boundary conditions in MD simulations.

At the lipid–water interface the boundary conditions are the following:

$$\mathbf{n}\cdot\mathbf{j_i} = 0;\quad \mathbf{n}\cdot\varepsilon_0\varepsilon_e\nabla\Psi = -q_{surf};\quad \mathbf{v} = 0\,. \tag{9}$$

The zero flux for concentration simply implies that there is no flux of ions into the membrane. The boundary condition for electric potential describes the electric potential next to a surface with surface charge q_{surf} and imposes the requirement of electroneutrality. The no slip boundary condition for velocity implies that there is no fluid movement at the lipid–water interface. This is a typical boundary condition used for modeling electroosmotic flow and is argued by the fact that the interfacial water is immobilized next to a hydrophilic surface [76].

The value of the surface charge q_{surf} was extracted from the MD system using an approach described in Supplementary Material Section S2.3. As we explain in more detail in S2.3, representing the bound Na ions with simple two-dimensional surface charge in the FEM model is a rough approximation, hardly applicable at the molecular scale. Hence, we performed calculations for two values of the surface charge (0.20 q_e/nm^2 and 0.27 q_e/nm^2), which were the most reasonable according to our approach of data extraction.

In simplified variants of the FEM model we omit the Navier–Stokes equation, set the fluid velocity to 0 m/s (model with surface charge only — FEM model 2), and neglect the surface charge by setting $q_{surf} = 0$ q_e/nm^2 (model without surface charge and fluid flow — FEM model 1).

2.3.3. Calculation of pore conductance and selectivity

The electric current I_i through the pore due to Na and Cl ions is calculated by integrating the electric current density $\mathbf{J_i}$ over the pore's horizontal cross-sectional area (Fig. 1b) (we verified that the calculated current is invariant to the plane of integration). $\mathbf{J_i}$ is directly related to the molar flux $\mathbf{j_i}$ from the Nernst–Planck equation by $\mathbf{J_i} = Fz_i\mathbf{j_i}$, hence

$$I_i = \iint_{A_{pore}}\mathbf{J_i}\cdot d\mathbf{A} = F\ z_i.\iint_{A_{pore}}\mathbf{j_i}\cdot d\mathbf{A} \tag{10}$$

From the known electric current and transmembrane voltage U_m (which is imposed by boundary conditions), we can calculate the pore conductance for Na ions (G_{Na}), Cl ions (G_{Cl}), and the total pore conductance (G_{tot}), which is the sum of the former two.

$$G_{Na} = I_{Na}/U_m;\quad G_{Cl} = I_{Cl}/U_m;\quad G_{tot} = G_{Na} + G_{Cl}\,. \tag{11}$$

The selectivity of the pore is then defined as the ratio

$$S = G_{Cl}/G_{Na}. \tag{12}$$

3. Results and discussion

The main intention of our study is to verify whether the Poisson–Nernst–Planck (PNP) theory can correctly predict the conductance of lipid pores. For this reason we developed three increasingly complex variants of our FEM model, the results of which are compared with results from MD simulations in the following sections.

3.1. Pore conductance

3.1.1. Basic PNP model

In the first stage of our FEM calculations of pore conductance we used the basic PNP model neglecting both the electric double layer and the electroosmotic fluid flow (FEM model 1). Results of the total

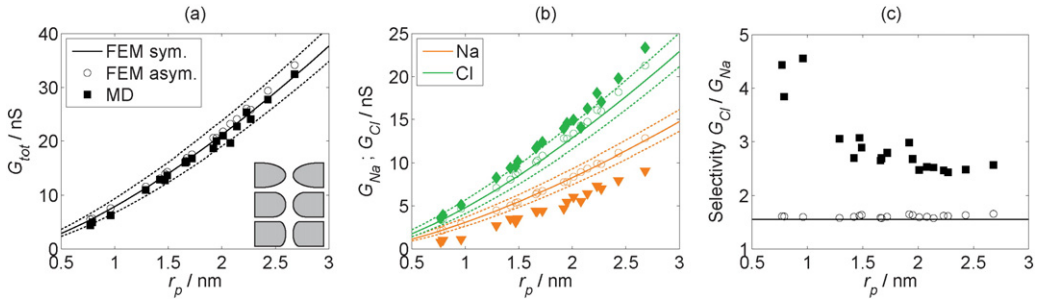

Fig. 3. Results obtained with the basic PNP model without surface charge and fluid flow (FEM model 1). Results from MD are shown in black squares (total pore conductance in (a) and selectivity in (c)), orange triangles (conductance for Na in (b)), and green diamonds (conductance for Cl in (b)). Results from the symmetric model are represented by solid lines and results from the asymmetric model with open circles. The dotted lines indicate results considering different pore shapes, which are shown at the bottom right corner in (a). The upper and lower dotted curve correspond to the uppermost and lowermost pore shape, respectively.)

pore conductance as obtained with the symmetric model (solid line) and asymmetric model (circles) are shown in Fig. 3 together with the results obtained from MD simulations (black squares in Fig. 3a). The agreement between the FEM model and MD results is quite remarkable considering that we are applying a continuum theory on a few nm large system. The difference in the results obtained with the symmetric and asymmetric model are only minor, and arise from the different box dimensions and from accounting for the concentration difference across the bilayer, which results in higher ionic concentration inside the pore of the asymmetric model. However, the difference is not due to diffusive current, as the latter is three orders of magnitude lower than the electrophoretic current (up to 0.4% of the total current as predicted by the FEM model).

Since we approximated the pore as perfectly toroidal, we in addition probed the influence of the pore shape on the calculated pore conductance. We represented the pore edge with an ellipse (with semiaxes ratio of 0.5 or 2) instead of a circle. The considered pore shapes are shown in a schematic at the bottom right corner of Fig. 3a, and the corresponding results are presented using dotted lines (Fig. 3a and b). The pore shape which resembles a cylindrical pore results in lower pore conductance; on the opposite, pore with more "egg-like" edges results in higher pore conductance. Notably, all data points from the MD system fall in between the results for different pore shapes and are indeed best represented by a toroidal shape, which also appears to be the best approximation according to ionic concentration profiles, later presented in Fig. 8.

Although the total pore conductance is very well described by the FEM model, the model does not predict correctly the conductance for Na and Cl ions separately, regardless of the pore shape considered (Fig. 3b). Consequently, the model is also not able to reproduce the selectivity of the pore for Cl ions, as was observed in MD simulations (Fig. 3c). The selectivity of 1.5 obtained with the FEM model is equal to the ratio of Cl and Na diffusion coefficients. Apart from the difference in the diffusion coefficients, there is nothing else incorporated in the FEM model that would invoke higher selectivity, and especially, not its dependence on the pore radius. Particularly interesting is that according to MD results, the selectivity for larger pores asymptotically approaches ~2.6 and not 1.5 as would be predicted by the FEM model. Obviously, there is something missing in the model to reproduce such result. Even more important is the question, how can the model reproduce the overall pore conductance, if it cannot properly describe the current of Na and Cl ions flowing through the pore? In the present case, the reason lies in the fact that the model underpredicts the conductance for Cl ions and overpredicts the conductance for Na ions in a similar way. However, at this stage we cannot be certain whether this is simply a coincidence, and whether the FEM model would completely fail to predict the total pore conductance in another situation.

According to the knowledge gained from ion channels and nanochannels, the selectivity for particular type of ions can be due to one or more of the following reasons:

- different ion mobility (diffusion coefficient) inside the channel/pore [48,63,84],
- size exclusion (ions, which are too large and cannot enter the channel/pore) [60,61,64,66,85],
- electrostatic exclusion (channels/pores with charged inner surface will favor the presence of counterions and exclude coions) [60,61,63,66,85], and
- fluid motion, which enhances the current of ions with one charge and opposes the current of ions of the opposite charge (depending on the direction of the fluid movement) [73].

We already observed that there is a difference in the diffusion coefficient of Na and Cl ions in the bulk phase. To corroborate our calculation of the diffusion coefficients from the mean squared displacement of ion positions, we also independently calculated the diffusion coefficients from the autocorrelation functions of ion positions as described by Hummer [86] and applied by Vorobyov et al. [87], and obtained similar results (data not shown). Therefore we are confident that the estimates of diffusion coefficients in the bulk are robust. Nevertheless, there could be an additional reduction of the diffusion coefficient (for free ions) inside a confined pore [48,63,84]. However, it is not expected that the diffusion coefficient for Cl ions is increased, as would be required to reproduce the conductance for Cl ions in Fig. 3b. If there is a reduction in the diffusion coefficients, the FEM model should systematically overpredict the calculated pore conductance for both Na and Cl ions.

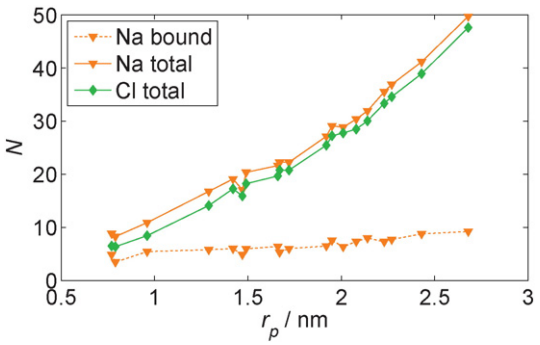

Fig. 4. Number of ions inside the pore. The number was extracted from each 20 ns long part of the trajectories by counting the number of ions in a 2 nm high central region of the pore.

Size exclusion of Na ions in our MD system is unlikely, as the pores are larger (radius ≥ 0.8 nm) than the radius of Na ions imposed by the CHARMM36 force field used in the MD system (0.27 nm). We can also corroborate this by counting the number of ions inside the pore. Fig. 4 shows that inside the pore there is always a slightly higher number of Na than Cl ions. Size exclusion is hence not responsible for pore selectivity.

Fig. 4 also demonstrates that the higher number of Na ions in the pore is due Na ions bound to the lipid headgroups, which effectively acts as positive surface charge on the pore wall. Electrostatic exclusion should therefore contribute to the pore selectivity for mobile Cl ions, by making the environment energetically favorable for negative charges.

In addition, as we already explained in Section 2.2, the net fluid movement observed in the MD simulations could notably contribute to the pore selectivity as it enhances the current of Cl ions and reduces the current of Na ions.

Taking into account the above considerations, we upgraded the FEM model: in the first stage, we added a surface charge to the lipid–water interface representing bound Na ions (FEM model 2), and in the second stage we included in addition a description for the fluid flow (FEM model 3).

3.1.2. PNP model with surface charge and fluid flow

The results obtained with the model including surface charge are presented in Fig. 5. Similarly as we observed in Fig. 3, the results from the symmetric and asymmetric models yield comparable results, therefore we only present the results obtained with the symmetric model. Calculations were performed for two values of surface charge, namely 0.20 q_e/nm^2 and 0.27 q_e/nm^2, and we also present the results from FEM model 1 without surface charge (from Fig. 3) for comparison. Including surface charge into the model increases the conductance of the pore for Cl ions, whereas it reduces the conductance for Na ions, but to a lesser extent (Fig. 5b). Consequently, the total pore conductance is slightly higher than predicted by the model without surface charge, yet very close to the results obtained with the MD system (Fig. 5a). The predicted selectivity for Cl ions (Fig. 5c) is much better represented; the FEM model 2 with surface charge is able to recover the dependence of the selectivity on the pore radius as well as selectivity higher than predicted simply from the ratio of diffusion coefficients.

The agreement between the FEM model and the MD results is though not yet perfect. Particularly from Fig. 5b we can see that the FEM model still considerably overpredicts the conductance for Na ions. Moreover, further increase in the surface charge would not decrease the Na conductance as the results for both values of the surface charge practically overlap.

An additional mechanism that reduces the Na conductance can be attributed to the electroosmotic fluid flow, as is demonstrated in Fig. 6. Including both the surface charge and the fluid flow in the FEM model 3 (still) correctly predicts the total pore conductance, and in addition also reproduces the pore conductance for Na and Cl ions and the pore selectivity much better than the basic FEM model 1 (Fig. 3). Further argument that both surface charge and fluid flow need to be incorporated in the model to obtain such agreement is given by the results for selectivity in the case of zero surface charge (Fig. 6c, solid line). The fluid flow itself cannot correctly reproduce neither the dependence of the selectivity on the pore radius, nor the value of selectivity for the largest pores. In addition to the results obtained with the symmetric model, we show also the selectivity obtained with the asymmetric model by circles in Fig. 6c, where the largest circles correspond to results with zero surface charge and the smallest circles to results obtained with the highest surface charge. In accordance with results shown in Fig. 3, the asymmetric model yields similar results as the symmetric model. This further confirms that the bound Na ions and the electroosmotic fluid flow are the most important properties for reproducing the pore selectivity for Cl ions, whereas the concentration and volume changes on either side of the bilayer resulting from the net water flow and finite size of the system have a lesser effect on the pore conductance. Note that the pore selectivity for Cl ions has been observed also in previous MD simulations of ionic conduction through stable pores in POPC bilayer, which was attributed to the binding interactions of Na ions with the lipid headgroups [45]; however, the possible role of electroosmotic fluid flow was not discussed.

3.2. Electric potential and ionic concentration profiles

An additional way to verify whether the FEM model correctly presents the MD system is by comparing the profiles of the electric potential and ionic concentrations. Fig. 7 shows the electric potential profiles for pores with two sizes (with radius 0.8 nm and 1.5 nm). For the MD system, the profiles are shown for the region that was modeled with the FEM model. For the FEM model, the profiles are shown for the asymmetric model with surface charge and fluid flow. Similar profiles were also obtained with other models and are thus not presented. The agreement between the MD system and the FEM model is good, both implying that the highest electric potential gradient is present in the pore and hence most of the transmembrane voltage drops over the pore region. Note that the FEM model does not include the lipid bilayer, therefore the areas corresponding to it are white. The electric potential in the lipid region in the MD system is rather high due to the electric potential arising from the lipid dipoles, which is counterbalanced by the water dipoles, none included in the FEM model.

The profiles of ionic concentration are presented in Fig. 8, where only one half of the system is shown, with the center of the pore at coordinates (0, 0). Here we present both the results from the basic FEM model (FEM model 1), as well as the results from the model including the surface charge and fluid flow (FEM model 3). Note that the agreement is much better for FEM model 3, which can quite well reproduce the concentration of Na and Cl ions in the vicinity of the pore. This additionally confirms that FEM model 3 better represents the MD system than the basic FEM model, as was already argued by comparing the results for the pore selectivity.

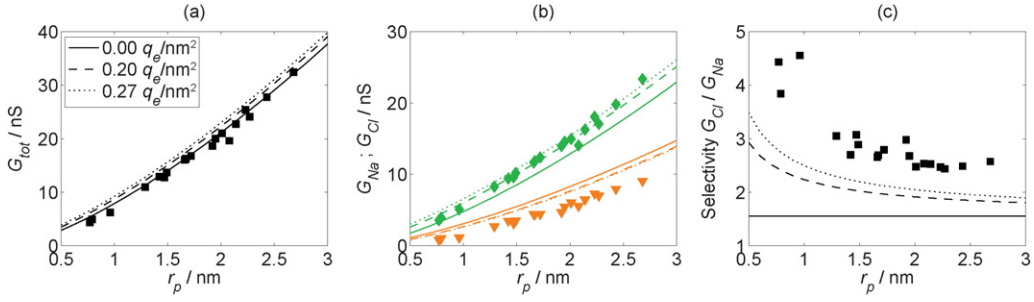

Fig. 5. Results obtained with the PNP model with surface charge and without fluid flow (FEM model 2). Apart from results for different surface charge, which are presented with solid, dashed and dotted lines (see legend in (a)), the notation is the same as in Fig. 3.

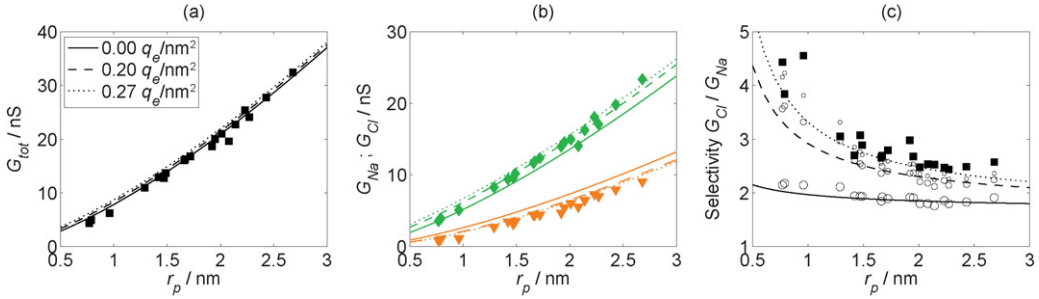

Fig. 6. Results obtained with the PNP model with surface charge and fluid flow (FEM model 3). Notation is the same as in Fig. 5.

Nonetheless, in all of the FEM models considered, the prediction of the total pore conductance is always very close to the one obtained from MD simulations. Including a description of the electric double layer and fluid flow has a counterbalancing effect on the electric current from Na and Cl ions. Both act to increase the current of Cl ions, and at the same time decrease the current of Na ions. This keeps the overall pore conductance very similar in all models considered.

According to our analysis we can make two summarizing conclusions. (i) FEM model 1 which neglects the electric double layer and the electroosmotic fluid flow (as is generally done for predicting ionic conduction through lipid pores) is not sufficient to describe the ionic currents for Na and Cl ions separately and consequently cannot describe the pore selectivity. Therefore, when one is interested in predicting the pore selectivity, it is necessary to take into account both the electric double layer and the electroosmotic fluid flow. (ii) The total pore conductance is not significantly influenced by the electric double layer and the electroosmotic fluid flow (at least not under the conditions probed in the MD simulations). Therefore, when one is interested in calculating the total pore conductance only, FEM model 1 is sufficient. This is relevant for experimental studies on planar lipid bilayers, where the pore size is extracted from measurements of the total pore conductance [37–39]. It is also relevant for continuum electroporation models, where only the theoretical expression for the total pore conductance is embedded in the models (and not for the separate ionic species in the electrolyte surrounding the pore) [19,25,28,88]. Since the total pore conductance is directly proportional to the bulk conductivity of the solution, which can be measured experimentally, the model can be further simplified to describe the solution in terms of its conductivity rather than ionic concentrations, as was done in [35,54].

Note, however, that FEM model 1 is still more complex than typical models of lipid pore conductance considered in previous studies, in particular regarding the pore shape, which is most often approximated as cylindrical. In the next section we discuss the applicability of different simplified analytical derivations of pore conductance.

3.3. Applicability of simplified analytical derivations of pore conductance

Since analytical description is difficult or even impossible to obtain for complex pore shapes and complex electrolyte solutions, most derivations were performed by approximating the pore shape as cylindrical and considering a binary electrolyte (composed of only one cationic and one anionic species) [52–54]. Early derivations also assumed that the ions in the pore flow only in the direction parallel to the central axis of the pore, thereby deriving the current–voltage relationship based on one-dimensional equations. Indeed, the most recent derivation of pore conductance performed by Li and Lin [54] demonstrated that for cylindrical pores, such approximation is valid. The general analytical description for conductance of a cylindrical pore is

$$G_p = \frac{I_p}{U_m} = \frac{1}{R_{spd} + R_{int}} = \frac{2\pi\sigma_e {r_p}^2}{\pi r_p + 2d_m} \tag{13a}$$

$$R_{spd} = \frac{1}{2\sigma_e r_p} \tag{13b}$$

$$R_{int} = \frac{d_m}{\sigma_e \pi {r_p}^2} \tag{13c}$$

where r_p is the pore radius, and σ_e is the conductance of the electrolyte inside the pore. When the conductivities of the electrolyte solutions on either side of the membrane are different, σ_e needs to be replaced by an effective conductivity of the solution inside the pore [54]. R_{spd} is the spreading (also access or input) resistance and accounts for the voltage drop at the pore entrance, whereas R_{int} is the resistance of the pore interior region and accounts for the voltage drop across the central region of the pore.

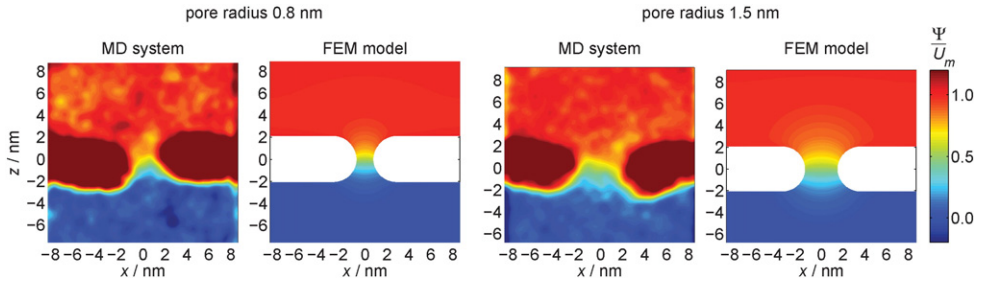

Fig. 7. Electric potential profiles from the MD system and the FEM model with surface charge and fluid flow (FEM model 3). The electric potential Ψ was normalized to the transmembrane voltage U_m. The profiles from the MD system were obtained based on an average over 20 ns long parts of the trajectory (see also Supplementary Material, Section S2.7).

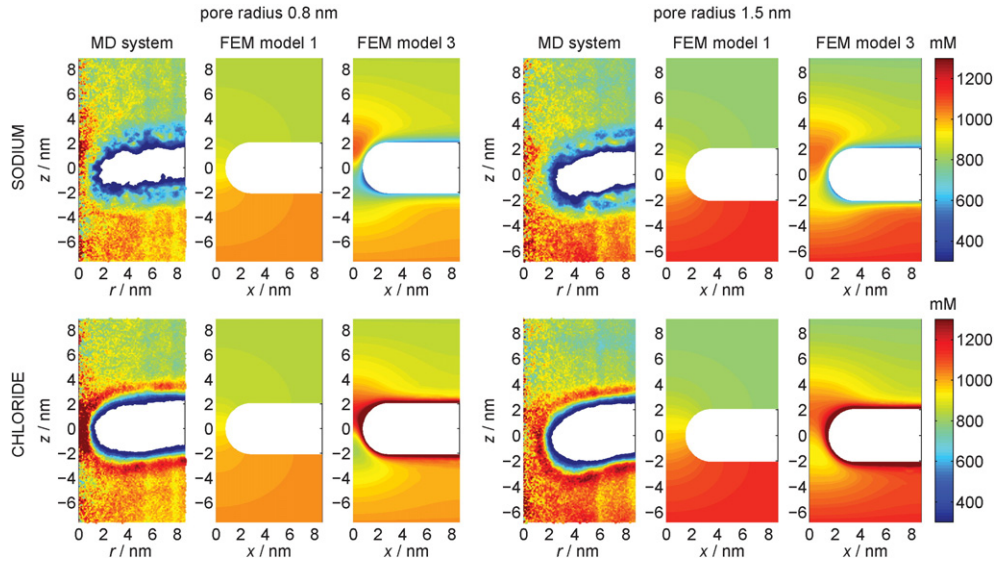

Fig. 8. Na and Cl concentration profiles from the MD system and the basic FEM model without surface charge and fluid flow (FEM model 1), and from the FEM model with surface charge and fluid flow (FEM model 3). The concentration profiles from MD system were obtained in the same way as in Fig. 2c (see also Supplementary Material, Section S2.8).

3.3.1. Estimation of pore radius from experimental measurements of lipid bilayer conductance

Analytical descriptions were also used for extraction of pore size based on conductance measurements on planar lipid bilayers. In certain experimental studies, the spreading resistance was neglected and only the resistance of the pore interior region was taken into account [37–39]. Fig. 9 compares different descriptions of pore conductance. Since the pore conductance depends linearly on the electrolyte conductivity σ_e, we normalized the total pore conductance by σ_e. On the left-hand side the normalized conductance is shown for pore radii up to 3 nm along with the results from MD simulations and the symmetric FEM model 1, already presented in previous sections. In addition we also show the conductance of a toroidal pore, assuming that the source of the electric potential is infinitely far away from the pore (black dotted line), which is related to the way how the conductance of cylindrical pores (gray solid line) was derived [54]. Note that the toroidal shape results in moderately higher pore conductance at small radii (Fig. 9, left), but basically overlaps with the conductance of cylindrical pores for large pore radii (Fig. 9, right), where the spreading resistance has the dominant contribution, as is also corroborated by experiments [89]. The description of pore conductance neglecting the spreading resistance (gray dotted line), however, results in different (purely quadratic) dependence on the pore radius, which is in disagreement with results from MD simulations. Moreover, when the spreading resistance is neglected, the pore conductance is considerably overestimated for larger pores. Hence, assuming that the pore conductance can simply be approximated as the conductance of its interior region is an oversimplification for pores of practically any size. The studies, which reported estimates of pore size as calculated from conductance measurements and (13c), therefore underestimated the pore radii.

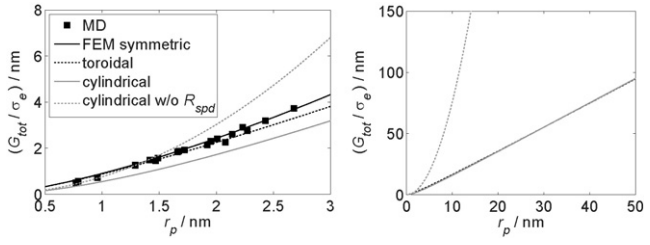

Fig. 9. Comparison of analytical descriptions of pore conductance. Pore conductance was normalized by the conductivity of electrolyte solution σ_e. Left graph shows the normalized pore conductance for pore radius up to 3 nm, and the right graph for pore radius up to 50 nm. "MD" and "FEM symmetric" are the results from MD simulations and the symmetric FEM model 1, as described in previous section. "Toroidal" shows our numerical result for a toroidal pore shape, but with the dimensions of the electrolyte region of the model much larger than the pore dimensions (as though the source of the electric potential was infinitely far away from the pore). "Cylindrical" and "cylindrical w/o R_{spd}" show normalized pore conductance as calculated by Eqs. (13a) and (13c), respectively.

In Supplementary Material, Table S3, we gathered the measurements of pore conductance from different experimental studies along with the reported estimates of the pore radius, which were obtained using simplified analytical expressions. We then recalculated the pore radius using the PNP model with a toroidal pore. We observed that the errors of the reported estimates can reach from a fraction of nm (for small pores) to more than 100 nm (for large pores). The list of experimental results (Table S3) also shows that the size of the pores, observed in our MD simulations, is on the lower edge of the ones reported is the literature, but overall in agreement with experiment.

We need to mention that conductance of single pores can be experimentally determined by measuring the conductance of planar lipid membranes (also called black lipid membrane, BLM), but only under specific experimental conditions. Namely, when a constant voltage is applied across a lipid membrane, the electroporation theory predicts that multiple pores form simultaneously, which do not have the same size but rather a size distribution [18]. A study by Melikov et al. [90] though showed that constant voltage can be applied across a BLM to directly characterize single pores when using the patch clamp technique. Measurements at constant or linearly rising electric current provide a better approach, where the fluctuations in transmembrane voltage appearing at moderate enforced currents can be attributed to size fluctuations of single pores [37–40]. Nonetheless, the possibility that the measured conductance in such experiments results from multiple pores cannot be completely excluded.

In cases where multiple pores are expected to form in the membrane, whether in simple lipid systems or in cell membranes, the measured membrane conductance needs to be analyzed in terms of an electroporation model describing the dynamics of the electroporation process, including the kinetics of pore formation and variations of the pore size under the influence of the transmembrane voltage [24,25]. In the next section we address the effect of using simplified

descriptions of pore conductance in electroporation models in greater detail.

3.3.2. Continuum electroporation models

As we already discussed in Introduction, the description of the pore conductance plays an important role in electroporation models, where different variants of analytical derivations for the conductance of a cylindrical pore are most often used. For example, apart from derivation given in Eq. (13) [30,54,31,28], certain authors also assumed that the movement of ions through the pore is hindered because that the pore walls exert a drag force on ions due to the finite size of ions (the steric hindrance) [24,91,33], and/or because an ion has to overcome an energetic barrier (the Born energy) arising from repulsive image forces in the low dielectric pore wall [25,33,52,53,88,91].

In this section we present an example of how different descriptions of pore conductance can affect the results of an electroporation model. Our intention is not to make an extensive analysis, but rather to make a statement that correct description of pore conductance will become increasingly important in further development of electroporation models with the aim of using the models for quantitative rather than qualitative predictions. The electroporation model we used was adapted from [91], the details of which are given in the Supplementary Material Section S4.

In the electroporation model we considered four descriptions of pore conductance: (i) numerically calculated conductance of a toroidal pore (this study); (ii) analytical derivation for conductance of a cylindrical pore based on the PNP theory (Eq. (13) [54]); (iii) analytical derivation for conductance of a cylindrical pore taking into account the Born energy and steric hindrance [91]; and (iv) analytical derivation for conductance of a cylindrical pore, neglecting the spreading resistance, but taking into account the Born energy of ions [25,88]. Fig. 10 shows the time evolution of the relative increase in the membrane conductance (which arises from formation of multiple pores in the membrane) and the mean pore radius during and after application of a single electroporative 100 μs pulse. The results demonstrate that the descriptions of pore conductance including the Born energy (indicated with B in brackets in the legend of Fig. 10) predict about an order of magnitude lower membrane conductance after the pulse (Fig. 10a), as well as lower mean pore radius during the pulse (Fig. 10b). The description of pore conductance also affects the calculated number of pores, and the fractional area of pores in the membrane, the latter sometimes used to describe the transport of molecules across the membrane [31,32] (data not shown). In addition, the influence of the description of the pore conductance is quantitatively and in certain cases qualitatively different for different pulse parameters (data not shown).

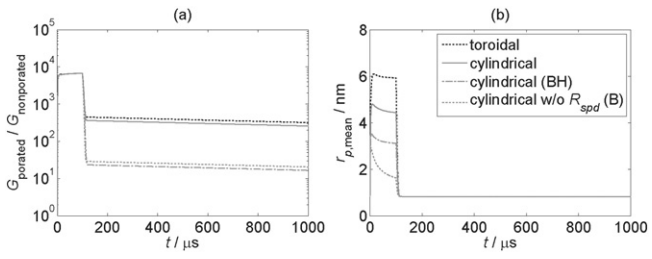

Fig. 10. Results obtained with electroporation model using four different descriptions of pore conductance: (i) numerically calculated conductance of a toroidal pore (black dotted line); (ii) analytical derivation for conductance of a cylindrical pore based on the PNP model (gray solid line); (iii) analytical derivation for conductance of a cylindrical pore taking into account the Born energy and steric hindrance (gray dash-dotted line); and (iv) analytical derivation for conductance of a cylindrical pore, neglecting the spreading resistance, but taking into account the Born energy of ions (gray dotted line). The graphs show the time evolution of the relative increase in the membrane conductance (a) and mean pore radius (b) during and after application of an electroporative 100 μs pulse.

If the movement of an ion across the pore is hindered due its interactions with the pore wall, the diffusion coefficient of the ion inside the pore becomes reduced. Comparisons of experimental results with theoretical studies on narrow ion channels showed that this reduction needs to be taken into account in the PNP models [63]. Such reduction of diffusion coefficients has also been considered for theoretically describing the conductance of lipid pores [48,91]. In our model, however, we simply used the values of bulk ionic diffusion coefficients, and did not consider any reduced diffusion of ions within the pore. Good agreement between our PNP model and results from MD simulations suggests that the majority of ions translocating through the pore do not feel considerable hindrance effects. We attribute this to the fact that the ions are smaller than the pores in our simulations and that a lipid pore is more flexible and fluctuating in size compared to an ion channel. Note also that the average number of bound Na ions (which obviously move in a hindered way) was in the model represented by immobile surface charge which does not contribute to the ionic current.

The Born energy (self-dielectric energy) of ions needs to be added to the PNP theory when only a single or very few ions are found in the pore at a certain moment and the electrolytic shielding in the pore is not effective [62]. According to our MD simulations, this is not the case, as multiple ions are continuously present inside the pore (Fig. 4). Furthermore, we observed no measurable influence of the transmembrane voltage on the conductance of pores with similar radius in MD simulations, which further confirms that the Born energy, which is reduced by the transmembrane voltage, does not affect the pore conductance in the MD system. The Born energy, however, may be important in the case of very low conductive electrolyte solutions, when much less ions are present in the electrolyte.

Finally we need to stress that we tested the PNP theory for describing the pore conductance only in the case of 1 M NaCl solution, where the Debye length (~0.3 nm) is shorter than the smallest pore radius (~0.8 nm). In such case, the predictions of the PNP theory were already found comparable to Brownian dynamics simulations of ion conduction through ion channels [61]. Although 1 M salt concentration is often used in experiments with planar lipid bilayers [92], it is much higher than physiological ionic concentration of ~0.15 M. Further investigations could therefore be performed by investigating the pore conductance at lower ionic concentrations, different ionic concentrations on each side of the bilayer, in the presence of other ionic species, and on bilayers with different lipid compositions, either using MD simulations as performed here, or less computationally demanding Brownian dynamics simulations [55,62,63].

4. Conclusions

In the present study we constructed a theoretical model of the pore conductance based on the continuum Poisson–Nernst–Planck (PNP) theory and compared the obtained results with results from molecular dynamics (MD) simulations. We developed an approach to relate the continuum model to the system in MD simulations by directly extracting all relevant model parameters from the MD system. Our analysis demonstrates that the pore selectivity (higher conductance of the pore for Cl than to Na ions) is mediated by the electric double layer, which forms at the lipid–water interface, and the electroosmotic fluid flow through the pore. When both are taken into account, the PNP model correctly (quantitatively) predicts the ionic currents for Cl and Na ions and by that also the pore selectivity. The total pore conductance is though not considerably affected neither by the electric double layer nor the electroosmotic fluid flow. We further demonstrate that correct description of the pore conductance is important when extracting the pore size from experimental measurements as well as when using continuum electroporation models. Among the existing analytical descriptions of the pore conductance, the derivation for the conductance of a cylindrical pore [54] seems to be the closest to the results obtained with MD simulations. However, approximating the pore shape as

cylindrical underpredicts the pore conductance for pores with radii up to few nm, whereas modeling the pore shape as toroidal provides a better agreement with MD simulations. Overall we can conclude that the PNP theory is sufficient to describe conductance of lipid pores, at least for pores in symmetric zwitterionic lipid bilayers in the presence of ionic concentrations in 1 M range, for which the MD simulations were performed. In addition, our study demonstrates that continuum modeling can be efficiently used as complementary method to molecular scale models for investigating lipid pores.

Acknowledgments

L.R. and D.M. acknowledge the support from the Slovenian Research Agency (ARRS) under the program P2-0249 and funding for Junior Researchers R856. M.C. acknowledges the support of the "Istituto Italiano di Tecnologia" (IIT) under project 81/13 16-04-2013. M.T. acknowledges the support of the French Agence Nationale de la Recherche, under grant ANR-10_BLAN-916-03-INTCELL. Part of the study was performed during the Short Term Scientific Mission (STSM-TD1104-270215-057439) of L.R., which was granted by COST action TD1104 (www.electroporation.net). The study was conducted in the scope of the European Associated Laboratory for Pulsed Electric Field Applications in Biology and Medicine (LEA EBAM).

Appendix A. Supplementary data

Supplementary data to this article can be found online at http://dx.doi.org/10.1016/j.bioelechem.2016.03.005.

References

[1] R. Cannon, S. Ellis, D. Hayes, G. Narayanan, R.C.G. Martin 2nd, Safety and early efficacy of irreversible electroporation for hepatic tumors in proximity to vital structures, J. Surg. Oncol. 107 (2013) 544–549, http://dx.doi.org/10.1002/jso.23280.
[2] J. Teissié, Electrically mediated gene delivery: basic and translational concepts, in: M. Wei (Ed.), Nov. Gene Ther. Approaches, InTech, 2013http://dx.doi.org/10.5772/54780.
[3] M.L. Yarmush, A. Golberg, G. Serša, T. Kotnik, D. Miklavčič, Electroporation-based technologies for medicine: principles, applications, and challenges, Annu. Rev. Biomed. Eng. 16 (2014) 295–320, http://dx.doi.org/10.1146/annurev-bioeng-071813-104622.
[4] S. Lakshmanan, G.K. Gupta, P. Avci, R. Chandran, M. Sadasivam, A.E.S. Jorge, et al., Physical energy for drug delivery; poration, concentration and activation, Adv. Drug Deliv. Rev. 71 (2014) 98–114, http://dx.doi.org/10.1016/j.addr.2013.05.010.
[5] G. Sersa, J. Teissié, M. Cemazar, E. Signori, U. Kamensek, G. Marshall, et al., Electrochemotherapy of tumors as in situ vaccination boosted by immunogene electrotransfer, Cancer Immunol. Immunother. 64 (2015) 1315–1327, http://dx.doi.org/10.1007/s00262-015-1724-2.
[6] S. Toepfl, V. Heinz, D. Knorr, High intensity pulsed electric fields applied for food preservation, Chem. Eng. Process. Process Intensif. 46 (2007) 537–546, http://dx.doi.org/10.1016/j.cep.2006.07.011.
[7] P.Y. Phoon, F.G. Galindo, A. Vicente, P. Dejmek, Pulsed electric field in combination with vacuum impregnation with trehalose improves the freezing tolerance of spinach leaves, J. Food Eng. 88 (2008) 144–148, http://dx.doi.org/10.1016/j.jfoodeng.2007.12.016.
[8] S. Shayanfar, O. Chauhan, S. Toepfl, V. Heinz, The interaction of pulsed electric fields and texturizing–antifreezing agents in quality retention of defrosted potato strips, Int. J. Food Sci. Technol. 48 (2013) 1289–1295, http://dx.doi.org/10.1111/ijfs.12089.
[9] M. Sack, J. Sigler, S. Frenzel, C. Eing, J. Arnold, T. Michelberger, et al., Research on industrial-scale electroporation devices fostering the extraction of substances from biological tissue, Food Eng. Rev. 2 (2010) 147–156, http://dx.doi.org/10.1007/s12393-010-9017-1.
[10] S. Mahnič-Kalamiza, E. Vorobiev, D. Miklavčič, Electroporation in food processing and biorefinery, J. Membr. Biol. 247 (2014) 1279–1304, http://dx.doi.org/10.1007/s00232-014-9737-x.
[11] M.D.A. Zbinden, B.S.M. Sturm, R.D. Nord, W.J. Carey, D. Moore, H. Shinogle, et al., Pulsed electric field (PEF) as an intensification pretreatment for greener solvent lipid extraction from microalgae, Biotechnol. Bioeng. 110 (2013) 1605–1615, http://dx.doi.org/10.1002/bit.24829.
[12] C. Gusbeth, W. Frey, H. Volkmann, T. Schwartz, H. Bluhm, Pulsed electric field treatment for bacteria reduction and its impact on hospital wastewater, Chemosphere 75 (2009) 228–233, http://dx.doi.org/10.1016/j.chemosphere.2008.11.066.
[13] C. Liu, X. Xie, W. Zhao, N. Liu, P.A. Maraccini, L.M. Sassoubre, et al., Conducting nanosponge electroporation for affordable and high-efficiency disinfection of bacteria and viruses in water, Nano Lett. 13 (2013) 4288–4293, http://dx.doi.org/10.1021/nl402053z.
[14] J. Teissié, M. Golzio, M.P. Rols, Mechanisms of cell membrane electropermeabilization: a minireview of our present (lack of ?) knowledge, Biochim. Biophys. Acta Gen. Subj. 1724 (2005) 270–280, http://dx.doi.org/10.1016/j.bbagen.2005.05.006.
[15] P.T. Vernier, Z.A. Levine, M.A. Gundersen, Water bridges in electropermeabilized phospholipid bilayers, Proc. IEEE 101 (2013) 494–504, http://dx.doi.org/10.1109/JPROC.2012.2222011.
[16] Y. Hu, S.K. Sinha, S. Patel, Investigating hydrophilic pores in model lipid bilayers using molecular simulations: correlating bilayer properties with pore-formation thermodynamics, Langmuir 31 (2015) 6615–6631, http://dx.doi.org/10.1021/la504049q.
[17] L.H. Wegner, W. Frey, A. Silve, Electroporation of DC-3F cells is a dual process, Biophys. J. 108 (2015) 1660–1671, http://dx.doi.org/10.1016/j.bpj.2015.01.038.
[18] J.C. Weaver, Y.A. Chizmadzhev, Theory of electroporation: a review, Bioelectrochem. Bioenerg. 41 (1996) 135–160, http://dx.doi.org/10.1016/S0302-4598(96)05062-3.
[19] M. Schmeer, T. Seipp, U. Pliquett, S. Kakorin, E. Neumann, Mechanism for the conductivity changes caused by membrane electroporation of CHO cell-pellets, Phys. Chem. Chem. Phys. 6 (2004) 5564–5574, http://dx.doi.org/10.1039/B411037D.
[20] A.A. Gurtovenko, J. Anwar, I. Vattulainen, Defect-mediated trafficking across cell membranes: insights from in silico modeling, Chem. Rev. 110 (2010) 6077–6103, http://dx.doi.org/10.1021/cr1000783.
[21] N.J. English, C.J. Waldron, Perspectives on external electric fields in molecular simulation: progress, prospects and challenges, Phys. Chem. Chem. Phys. 17 (2015) 12407–12440, http://dx.doi.org/10.1039/C5CP00629E.
[22] H. Pera, J.M. Kleijn, F.A.M. Leermakers, On the edge energy of lipid membranes and the thermodynamic stability of pores, J. Chem. Phys. 142 (2015) 034101, http://dx.doi.org/10.1063/1.4905260.
[23] I.G. Abidor, V.B. Arakelyan, L.V. Chernomordik, Y.A. Chizmadzhev, V.F. Pastushenko, M.P. Tarasevich, Electric breakdown of bilayer lipid membranes: I. The main experimental facts and their qualitative discussion, J. Electroanal. Chem. Interfacial Electrochem. 104 (1979) 37–52, http://dx.doi.org/10.1016/S0022-0728(79)81006-2.
[24] A. Barnett, J.C. Weaver, Electroporation: a unified, quantitative theory of reversible electrical breakdown and mechanical rupture in artificial planar bilayer membranes, Bioelectrochem. Bioenerg. 25 (1991) 163–182, http://dx.doi.org/10.1016/0302-4598(91)87001-W.
[25] K.A. DeBruin, W. Krassowska, Modeling electroporation in a single cell. I. Effects of field strength and rest potential, Biophys. J. 77 (1999) 1213–1224, http://dx.doi.org/10.1016/S0006-3495(99)76973-0.
[26] T.R. Gowrishankar, A.T. Esser, Z. Vasilkoski, K.C. Smith, J.C. Weaver, Microdosimetry for conventional and supra-electroporation in cells with organelles, Biochem. Biophys. Res. Commun. 341 (2006) 1266–1276, http://dx.doi.org/10.1016/j.bbrc.2006.01.094.
[27] M.E. Mezeme, G. Pucihar, M. Pavlin, C. Brosseau, D. Miklavčič, A numerical analysis of multicellular environment for modeling tissue electroporation, Appl. Phys. Lett. 100 (2012) 143701, http://dx.doi.org/10.1063/1.3700727.
[28] J. Li, W. Tan, M. Yu, H. Lin, The effect of extracellular conductivity on electroporation-mediated molecular delivery, Biochim. Biophys. Acta 1828 (2013) 461–470, http://dx.doi.org/10.1016/j.bbamem.2012.08.014.
[29] G. Pucihar, D. Miklavcic, T. Kotnik, A time-dependent numerical model of transmembrane voltage inducement and electroporation of irregularly shaped cells, IEEE Trans. Biomed. Eng. 56 (2009) 1491–1501, http://dx.doi.org/10.1109/TBME.2009.2014244.
[30] W. Krassowska, P.D. Filev, Modeling electroporation in a single cell, Biophys. J. 92 (2007) 404–417, http://dx.doi.org/10.1529/biophysj.106.094235.
[31] J. Li, H. Lin, Numerical simulation of molecular uptake via electroporation, Bioelectrochemistry 82 (2011) 10–21, http://dx.doi.org/10.1016/j.bioelechem.2011.04.006.
[32] D. Miklavčič, L. Towhidi, Numerical study of the electroporation pulse shape effect on molecular uptake of biological cells, Radiol. Oncol. 44 (2010) 34–41, http://dx.doi.org/10.2478/v10019-010-0002-3.
[33] K.C. Smith, R.S. Son, T.R. Gowrishankar, J.C. Weaver, Emergence of a large pore subpopulation during electroporating pulses, Bioelectrochemistry 100 (2014) 3–10, http://dx.doi.org/10.1016/j.bioelechem.2013.10.009.
[34] L. Rems, M. Ušaj, M. Kandušer, M. Reberšek, D. Miklavčič, G. Pucihar, Cell electrofusion using nanosecond electric pulses, Sci. Rep. 3 (2013) 3382, http://dx.doi.org/10.1038/srep03382.
[35] J.C. Neu, K.C. Smith, W. Krassowska, Electrical energy required to form large conducting pores, Bioelectrochemistry 60 (2003) 107–114, http://dx.doi.org/10.1016/S1567-5394(03)00051-3.
[36] M. Hibino, H. Itoh, K. Kinosita, Time courses of cell electroporation as revealed by submicrosecond imaging of transmembrane potential, Biophys. J. 64 (1993) 1789–1800.
[37] S. Kalinowski, G. Ibron, K. Bryl, Z. Figaszewski, Chronopotentiometric studies of electroporation of bilayer lipid membranes, Biochim. Biophys. Acta Biomembr. 1369 (1998) 204–212, http://dx.doi.org/10.1016/S0005-2736(97)00222-8.
[38] S. Koronkiewicz, S. Kalinowski, K. Bryl, Programmable chronopotentiometry as a tool for the study of electroporation and resealing of pores in bilayer lipid membranes, Biochim. Biophys. Acta Biomembr. 1561 (2002) 222–229, http://dx.doi.org/10.1016/S0005-2736(02)00347-4.
[39] M. Kotulska, J. Basalyga, M.B. Derylo, P. Sadowski, Metastable pores at the onset of constant-current electroporation, J. Membr. Biol. 236 (2010) 37–41, http://dx.doi.org/10.1007/s00232-010-9285-y.
[40] P. Kramar, L. Delemotte, A.M. Lebar, M. Kotulska, M. Tarek, D. Miklavčič, Molecular-level characterization of lipid membrane electroporation using linearly rising current, J. Membr. Biol. 245 (2012) 651–659, http://dx.doi.org/10.1007/s00232-012-9487-6.
[41] R.P. Joshi, H. Qiu, Asymmetric conduction in biological nanopores created by high-intensity, nanosecond pulsing: inference on internal charge lining the membrane based on a model study, J. Appl. Phys. 118 (2015) 094701, http://dx.doi.org/10.1063/1.4929808.

[42] T.J. Piggot, D.A. Holdbrook, S. Khalid, Electroporation of the *E. coli* and *S. aureus* membranes: molecular dynamics simulations of complex bacterial membranes, J. Phys. Chem. B 115 (2011) 13381–13388, http://dx.doi.org/10.1021/jp207013v.
[43] A.A. Gurtovenko, A.S. Lyulina, Electroporation of asymmetric phospholipid membranes, J. Phys. Chem. B 118 (2014) 9909–9918, http://dx.doi.org/10.1021/jp5028355.
[44] M.L. Fernández, M. Risk, R. Reigada, P.T. Vernier, Size-controlled nanopores in lipid membranes with stabilizing electric fields, Biochem. Biophys. Res. Commun. 423 (2012) 325–330, http://dx.doi.org/10.1016/j.bbrc.2012.05.122.
[45] M.-C. Ho, M. Casciola, Z.A. Levine, P.T. Vernier, Molecular dynamics simulations of ion conductance in field-stabilized nanoscale lipid electropores, J. Phys. Chem. B 117 (2013) 11633–11640, http://dx.doi.org/10.1021/jp401722g.
[46] M. Casciola, M.A. Kasimova, L. Rems, S. Zullino, F. Apollonio, M. Tarek, Properties of lipid electropores I: molecular dynamics simulations of stabilized pores by constant charge imbalance, Bioelectrochemistry 109 (2016) 108–116, http://dx.doi.org/10.1016/j.bioelechem.2016.01.006.
[47] M. Szabo, M.I. Wallace, Imaging potassium-flux through individual electropores in droplet interface bilayers, Biochim. Biophys. Acta Biomembr. (2015)http://dx.doi.org/10.1016/j.bbamem.2015.07.009.
[48] M. Kotulska, W. Dyrka, P. Sadowski, Fluorescent methods in evaluation of nanopore conductivity and their computational validation, in: A.G. Pakhomov, D. Miklavčič, M.S. Markov (Eds.), Adv. Electroporation Tech. Biol. Med. CRC Press 2010, pp. 123–139.
[49] F. Salomone, M. Breton, I. Leray, F. Cardarelli, C. Boccardi, D. Bonhenry, et al., High-yield nontoxic gene transfer through conjugation of the CM18-Tat11 chimeric peptide with nanosecond electric pulses, Mol. Pharm. 11 (2014) 2466–2474, http://dx.doi.org/10.1021/mp500223t.
[50] J. Kapla, J. Wohlert, B. Stevensson, O. Engström, G. Widmalm, A. Maliniak, Molecular dynamics simulations of membrane–sugar interactions, J. Phys. Chem. B 117 (2013) 6667–6673, http://dx.doi.org/10.1021/jp402385d.
[51] M. Leguèbe, A. Silve, L.M. Mir, C. Poignard, Conducting and permeable states of cell membrane submitted to high voltage pulses: mathematical and numerical studies validated by the experiments, J. Theor. Biol. 360 (2014) 83–94, http://dx.doi.org/10.1016/j.jtbi.2014.06.027.
[52] A. Barnett, The current–voltage relation of an aqueous pore in a lipid bilayer membrane, Biochim. Biophys. Acta Biomembr. 1025 (1990) 10–14, http://dx.doi.org/10.1016/0005-2736(90)90184-P.
[53] S. Kakorin, E. Neumann, Ionic conductivity of electroporated lipid bilayer membranes, Bioelectrochemistry 56 (2002) 163–166, http://dx.doi.org/10.1016/S1567-5394(02)00040-3.
[54] J. Li, H. Lin, The current–voltage relation for electropores with conductivity gradients, Biomicrofluidics 4 (2010) 013206, http://dx.doi.org/10.1063/1.3324847.
[55] W. Im, B. Roux, Ion permeation and selectivity of OmpF porin: a theoretical study based on molecular dynamics, Brownian dynamics, and continuum electrodiffusion theory, J. Mol. Biol. 322 (2002) 851–869, http://dx.doi.org/10.1016/S0022-2836(02)00778-7.
[56] B. Roux, T. Allen, S. Bernèche, W. Im, Theoretical and computational models of biological ion channels, Q. Rev. Biophys. 37 (2004) 15–103, http://dx.doi.org/10.1017/S0033583504003968.
[57] Q. Zheng, G.-W. Wei, Poisson–Boltzmann–Nernst–Planck model, J. Chem. Phys. 134 (2011)http://dx.doi.org/10.1063/1.3581031.
[58] H. Daiguji, P. Yang, A. Majumdar, Ion transport in nanofluidic channels, Nano Lett. 4 (2004) 137–142, http://dx.doi.org/10.1021/nl0348185.
[59] S. Bhattacharyya, A.K. Nayak, Electroosmotic flow in micro/nanochannels with surface potential heterogeneity: an analysis through the Nernst–Planck model with convection effect, Colloids Surf. Physicochem. Eng. Asp. 339 (2009) 167–177, http://dx.doi.org/10.1016/j.colsurfa.2009.02.017.
[60] G. Moy, B. Corry, S. Kuyucak, S.H. Chung, Tests of continuum theories as models of ion channels. I. Poisson–Boltzmann theory versus Brownian dynamics, Biophys. J. 78 (2000) 2349–2363, http://dx.doi.org/10.1016/S0006-3495(00)76780-4.
[61] B. Corry, S. Kuyucak, S.-H. Chung, Tests of continuum theories as models of ion channels. II. Poisson–Nernst–Planck theory versus Brownian dynamics, Biophys. J. 78 (2000) 2364–2381, http://dx.doi.org/10.1016/S0006-3495(00)76781-6.
[62] B. Corry, S. Kuyucak, C. Shin-Ho, Dielectric self-energy in Poisson–Boltzmann and Poisson–Nernst–Planck models of ion channels, Biophys. J. 84 (2003) 3594–3606, http://dx.doi.org/10.1016/S0006-3495(03)75091-7.
[63] S.Y. Noskov, W. Im, B. Roux, Ion permeation through the α-hemolysin channel: theoretical studies based on Brownian dynamics and Poisson–Nernst–Plank electrodiffusion theory, Biophys. J. 87 (2004) 2299–2309, http://dx.doi.org/10.1529/biophysj.104.044008.
[64] D. Goulding, J.-P. Hansen, S. Melchionna, Size selectivity of narrow pores, Phys. Rev. Lett. 85 (2000) 1132–1135, http://dx.doi.org/10.1103/PhysRevLett.85.1132.
[65] D. Gillespie, M. Valiskó, D. Boda, Density functional theory of the electrical double layer: the RFD functional, J. Phys. Condens. Matter 17 (2005) 6609, http://dx.doi.org/10.1088/0953-8984/17/42/002.
[66] D. Gillespie, Energetics of divalent selectivity in a calcium channel: the ryanodine receptor case study, Biophys. J. 94 (2008) 1169–1184, http://dx.doi.org/10.1529/biophysj.107.116798.
[67] Y. Hyon, B. Eisenberg, C. Liu, A mathematical model for the hard sphere repulsion in ionic solutions, Commun. Math. Sci. 9 (2011) 459–475, http://dx.doi.org/10.4310/CMS.2011.v9.n2.a5.
[68] T.-C. Lin, B. Eisenberg, A new approach to the Lennard-Jones potential and a new model: PNP-steric equations, Commun. Math. Sci. 12 (2014) 149–173, http://dx.doi.org/10.4310/CMS.2014.v12.n1.a7.
[69] T.-C. Lin, B. Eisenberg, Multiple solutions of steady-state Poisson–Nernst–Planck equations with steric effects, Nonlinearity 28 (2015) 2053, http://dx.doi.org/10.1088/0951-7715/28/7/2053.
[70] M. Burger, B. Schlake, M.-T. Wolfram, Nonlinear Poisson–Nernst–Planck equations for ion flux through confined geometries, Nonlinearity 25 (2012) 961, http://dx.doi.org/10.1088/0951-7715/25/4/961.
[71] J.-L. Liu, B. Eisenberg, Numerical methods for a Poisson–Nernst–Planck–Fermi model of biological ion channels, Phys. Rev. E 92 (2015) 012711, http://dx.doi.org/10.1103/PhysRevE.92.012711.
[72] P. Atkins, J. de Paula, Physical Chemistry, nineth ed. W. H. Freeman, New York, 2009.
[73] M. Yang, X. Yang, K. Wang, Q. Wang, X. Fan, W. Liu, et al., Tuning transport selectivity of ionic species by phosphoric acid gradient in positively charged nanochannel membranes, Anal. Chem. 87 (2015) 1544–1551, http://dx.doi.org/10.1021/ac503813r.
[74] A.T. Conlis, S. Singer, Modeling electroosmotic flow in nanochannels, in: M. Ferrari, R. Bashir, S. Wereley (Eds.), BioMEMS Biomed. Nanotechnol. Springer US 2006, pp. 301–330.
[75] Y. Zhang, G. Wu, W. Si, J. Sha, L. Liu, Y. Chen, Retarding and manipulating of DNA molecules translocation through nanopores, Chin. Sci. Bull. 59 (2014) 4908–4917, http://dx.doi.org/10.1007/s11434-014-0655-1.
[76] R.H. Nilson, S.K. Griffiths, Influence of atomistic physics on electro-osmotic flow: an analysis based on density functional theory, J. Chem. Phys. 125 (2006) 164510, http://dx.doi.org/10.1063/1.2358684.
[77] V. Knecht, B. Klasczyk, Specific binding of chloride ions to lipid vesicles and implications at molecular scale, Biophys. J. 104 (2013) 818–824, http://dx.doi.org/10.1016/j.bpj.2012.12.056.
[78] L. Yan, X. Ji, W. Lu, Molecular dynamics simulations of electroosmosis in perfluorosulfonic acid polymer, J. Phys. Chem. B 112 (2008) 5602–5610, http://dx.doi.org/10.1021/jp7121449.
[79] S.H. Lee, J.C. Rasaiah, Molecular dynamics simulation of ion mobility. 2. Alkali metal and halide ions using the SPC/E model for water at 25 °C, J. Phys. Chem. 100 (1996) 1420–1425, http://dx.doi.org/10.1021/jp953050c.
[80] D. van der Spoel, P.J. van Maaren, H.J.C. Berendsen, A systematic study of water models for molecular simulation: derivation of water models optimized for use with a reaction field, J. Chem. Phys. 108 (1998) 10220–10230, http://dx.doi.org/10.1063/1.476482.
[81] J.B. Hasted, D.M. Ritson, C.H. Collie, Dielectric properties of aqueous ionic solutions. Parts I and II, J. Chem. Phys. 16 (1948) 1–21, http://dx.doi.org/10.1063/1.1746645.
[82] M.A. González, J.L.F. Abascal, The shear viscosity of rigid water models, J. Chem. Phys. 132 (2010) 096101, http://dx.doi.org/10.1063/1.3330544.
[83] B. Kirby, Micro- and Nanoscale Fluid Mechanics: Transport in Microfluidic Devices, 1. Paperback Ed., Reprint, Cambridge Univ. Press, Cambridge, 2013.
[84] A.B. Mamonov, M.G. Kurnikova, R.D. Coalson, Diffusion constant of K+ inside Gramicidin A: a comparative study of four computational methods, Biophys. Chem. 124 (2006) 268–278, http://dx.doi.org/10.1016/j.bpc.2006.03.019.
[85] W. Nonner, L. Catacuzzeno, B. Eisenberg, Binding and selectivity in L-type calcium channels: a mean spherical approximation, Biophys. J. 79 (2000) 1976–1992, http://dx.doi.org/10.1016/S0006-3495(00)76446-0.
[86] G. Hummer, Position-dependent diffusion coefficients and free energies from Bayesian analysis of equilibrium and replica molecular dynamics simulations, New J. Phys. 7 (2005) 34, http://dx.doi.org/10.1088/1367-2630/7/1/034.
[87] I. Vorobyov, T.E. Olson, J.H. Kim, R.E. Koeppe, O.S. Andersen, T.W. Allen, Ion-induced defect permeation of lipid membranes, Biophys. J. 106 (2014) 586–597, http://dx.doi.org/10.1016/j.bpj.2013.12.027.
[88] R.W. Glaser, S.L. Leikin, L.V. Chernomordik, V.F. Pastushenko, A.I. Sokirko, Reversible electrical breakdown of lipid bilayers: formation and evolution of pores, Biochim. Biophys. Acta 940 (1988) 275–287, http://dx.doi.org/10.1016/0005-2736(88)90202-7.
[89] C. Wilhelm, M. Winterhalter, U. Zimmermann, R. Benz, Kinetics of pore size during irreversible electrical breakdown of lipid bilayer membranes, Biophys. J. 64 (1993) 121–128, http://dx.doi.org/10.1016/S0006-3495(93)81346-8.
[90] K.C. Melikov, V.A. Frolov, A. Shcherbakov, A.V. Samsonov, Y.A. Chizmadzhev, L.V. Chernomordik, Voltage-induced nonconductive pre-pores and metastable single pores in unmodified planar lipid bilayer, Biophys. J. 80 (2001) 1829–1836, http://dx.doi.org/10.1016/S0006-3495(01)76153-X.
[91] Z. Vasilkoski, A.T. Esser, T.R. Gowrishankar, J.C. Weaver, Membrane electroporation: the absolute rate equation and nanosecond time scale pore creation, Phys. Rev. E 74 (2006) 021904, http://dx.doi.org/10.1103/PhysRevE.74.021904.
[92] P. Kramar, D. Miklavčič, M. Kotulska, A. Maček Lebar, Voltage- and current-clamp methods for determination of planar lipid bilayer properties, in: A. Iglič (Ed.), Adv. Planar Lipid Bilayers Liposomes, Academic Press 2010, pp. 29–69.